SCIENTIFIC REP RTS

Towards high-bandwidth organic photodetection based on pure active layer polarization

Louisa Reissig[1,2], Simon Dalgleish[1,3] & Kunio Awaga[1]

Organic photodetectors offer distinct advantages over their inorganic analogues, most notably through optical transparency and flexibility, yet their figures-of-merit still lag behind those of inorganic devices, and optimization strategies generally encounter a trade-off between device responsivity and bandwidth. Here we propose a novel photodetector architecture in which an organic photoactive semiconductor layer (S) is sandwiched between two thick insulating layers (I) that separate the semiconductor from the metallic contacts (M). In this architecture a differential photocurrent response is generated purely from the polarization of the active layer under illumination. Especially for an asymmetric MISIM design, where one insulating layer is a high-k ionic liquid I_{IL} and the other a low-k polymer dielectric I_p, the responsivity/bandwidth trade-off is broken, since the role of the I_{IL} in efficient charge separation is maintained, while the total device capacitance is reduced according to I_p. Thus the benefits of single insulating layer differential photodetectors (MISM) using either I_{IL} or I_p are combined in a single device. Further improvements in device performance are also demonstrated by decreasing the series resistance of the photoactive layer through semiconductor:metal blending and by operation under strong background light.

The importance of insulating materials in the advancement of organic photodiodes is often overshadowed by the plethora of literature devoted to the design and processing of the light harvesting organic semiconductor component(s) that serve as the locus of light to energy conversion in such devices[1,2]. However, insulators have played a pivotal role in performance enhancement both for solar cells and for photodetectors based on a 2-terminal photodiode structure. Applied as thin interlayers at the electrode/semiconductor interface, various insulating materials have been used to form selective contacts for both holes[3,4] and electrons[5–7], even for the same electrode material[7,8]. Insulators have also been used as blending partners with the semiconductor materials, leading to enhanced performance and operational stability from thicker active layer films, and thereby realizing truly plastic electronic devices[9,10]. Pertinent to photodetectors, which are generally operated under strong reverse bias, thin insulating interlayers have been shown to dramatically reduce the dark current in devices[11–13], which constitutes the dominant component to electronic noise[14,15] and, accordingly, such devices have shown impressive values of detectivity and noise-equivalent power - both important figures of merit for photodetector technology. However, in all these examples, the insulator component should be sufficiently thin, or sufficiently percolated by the semiconductor, to allow the passage of a DC current upon illumination. An alternative use of insulator interlayers is to act as a blocking dielectric to accumulate free carriers formed in the semiconductor layer upon photoexcitation, and to generate a transient photocurrent response due to capacitive charging/discharging of the thick insulator dielectric[16]. The bipolar current response to light on/off is similar to that of a voltage differentiator, but where the driving voltage is the photovoltage generated across the semiconductor layer[17]. While unsuitable for DC applications, such as solar cells, such differential photodetectors are highly applicable to AC devices such as optical signal receivers.

Previous work on differential photodetectors has independently demonstrated device bandwidths up to 1 MHz[18] and responsivities reaching 272 mA/W[19], by using low- or high-k dielectric insulators, respectively, as the interlayer between the semiconductor and a metal electrode in a metal/insulator/semiconductor/metal (MISM)

[1]Department of Chemistry and IRCCS, Nagoya University, Furo-cho, Chikusa, 464-8602, Nagoya, Japan. [2]Institute of Experimental Physics, Freie Universität Berlin, Arnimallee 14, 14195, Berlin, Germany. [3]Institute for Advanced Research, Nagoya University, Furo-cho, Chikusa, 464-8601, Nagoya, Japan. Correspondence and requests for materials should be addressed to L.R. (email: Louisa_Reissig@gmx.de) or K.A. (email: awaga@mbox.chem. nagoya-u.ac.jp)

device architecture. Typically, organic polymer dielectrics have served as representative low-k dielectrics, while ionic liquids (ILs) have been used for enhanced responsivity due to the large capacitance of the electric double layers (EDLs) that form at the ionic liquid interfaces, as well as the associated large electric field developed at the S/I_{IL} interface that can enhance charge separation in the semiconductor following photoexcitation[17]. However, a trade-off has existed in these figures of merit due to the constraints imposed on the single dielectric layer. This trade-off has been demonstrated by Hu *et al.* for MISM devices based on solid-state dielectrics[20], and while the ionic liquid-based devices have shown improved responsivities compared to solid-state devices, their bandwidths are significantly reduced[19] (*c.f.* Supplemental Fig. S2). While a high-k dielectric can accommodate more charge at the S/I interface, the non-negligible charging time of the semiconductor layer (with its own RC time constant) is slowed accordingly by the changing electric field from the insulator layer, which is slower for high-k dielectrics, thus permitting only mutually opposed optimization of responsivity or bandwidth[17].

In this article we demonstrate a strategy to break the responsivity/bandwidth trade-off in differential photo-detectors, exploiting the photocurrent enhancement observed in the IL based MISM devices while maintaining the bandwidth of the low-k polymer devices. Recognizing the fact that charge extraction at the M/S interface is not a prerequisite for differential photocurrent generation, we explored the use of an additional polymer insulator layer (I_P) introduced between the semiconductor layer and the electrode, yielding a device structure of $MI_{IL}SI_PM$. For such devices, the strong electric field at the S/I_{IL} interface is largely maintained, supporting efficient charge separation across the active layer, while the series capacitance of the device is significantly reduced according to I_P (since $1/C_{tot} \approx 1/C_P$ when $C_{IL} \gg C_P$), thus the bandwidth can be expected to approach that of MISM devices based on low-k dielectrics. In this architecture, the photocurrent response is generated purely by the polarization of the semiconductor layer under illumination, without carrier injection from the electrode(s), thereby eliminating contact resistance effects that can additionally reduce the bandwidth and the responsivity of MISM devices. By this method, the divergent optimization strategies for MISM photodetectors converge in a platform that exploits the advantages of both insulator layer functions.

For the purposes of this study, Sn(II)-2,3-naphthalocyanine (SnNPc) was used as the active semiconductor component due to its strong Q-band absorption centred around 850 nm, which is ideally placed for short distance fibre-optic communication. Despite its low charge carrier mobility ($\mu^+ \approx 5 \times 10^{-5}\,\text{cm}^2\text{V}^{-1}\text{s}^{-1}$), SnNPc has previously been shown to yield reasonable responsivities for single component semiconductor layers in IL-based MISM devices for a range of ionic liquids, such as *N*-(2-methoxyethyl)-*N*-methylpyrrolidinium tetrafluoroborate (MB) or trimethylpropylammonium bis(trifluoromethanesulfonyl)imide (TT), with sufficient stability to allow comparative studies[21]. Figure 1 illustrates the design of a typical $MI_{IL}SI_PM$ photocell used in this study ($M_1 = Ag$, $I_{IL} = MB$, $S = 50\,\text{nm}$ SnNPc, $I_P = 200\,\text{nm}$ Parylene-C (PC), $M_2 =$ indium tin oxide (ITO)), together with its representative photocurrent characteristics (a full description of device assembly and photocurrent measurements can be found in the Supporting Information). It should be noted that such IL-based devices can be constructed with ITO serving as both electrodes, which results in a visible-transparent photodetector with a maximum transmittance of 82% at 590 nm, and 41% at its responsivity maximum of 870 nm (for a 50 nm film of SnNPc), as shown in the transmittance spectrum and responsivity spectrum of Fig. 1b. Compared to the absorption spectrum of SnNPc (shaded area, Fig. 1b), the device transmittance shows greater attenuation for light at 780 nm due to scattering and/or interference effects through the various layers of the transparent device, which accounts for the suppressed photocurrent contribution of the blue shoulder of the Q-band absorption in the SnNPc film.

Similar to previous MISM photodetectors, the photocurrent response of the $MI_{IL}SI_PM$ devices show a characteristic progression with frequency of light signal (under square-wave modulated LED illumination), from a transient waveform at low frequencies (where complete capacitive charging of the device can be achieved), to become square-wave over a range of frequencies until the rise-time of the photoresponse is exceeded, whereupon the signal magnitude drops sharply (Fig. 1d). The device bandwidth (BW) can be calculated from the photocurrent rise time (τ_{rise}) as $BW = 0.35/\tau_{rise}$, which is shown to correspond well to the point at which the photocurrent response drops below 70% of that at square-wave[13], and which can be further improved by using a pulsed laser for device excitation (50% duty cycle), due to its smaller spot size (which yields a reduced geometric capacitance from a smaller active device area) (Fig. 1c). The $MI_{IL}SI_PM$ photodetectors are best compared to their $MI_{IL}SM$ analogues at square-wave where the responsivity becomes frequency independent[18], which occurs at ~1 MHz for $MI_{IL}SI_PM$ and ~10 kHz for $MI_{IL}SM$. While the bandwidth for $MI_{IL}SI_PM$ of 3.1 MHz is almost 100x larger than that of the analogous $MI_{IL}SM$ (31 kHz), its responsivity is smaller by only a factor of 1.2 (Fig. 1d). As a convenient metric, we introduce the responsivity-bandwidth product (RBP) (*c.f.* gain-bandwidth product) as a means to compare the devices. It is clear that, despite its reduced responsivity, the $MI_{IL}SI_PM$ device improves upon $MI_{IL}SM$ in this metric due to a significant improvement in its bandwidth, yielding a RBP of 290, compared to 3.5 for the $MI_{IL}SM$ device.

To demonstrate the generality of improvement in RBP of $MI_{IL}SI_PM$ over $MI_{IL}SM$, various device configurations were tested based on SnNPc as a single component semiconductor layer, as well as bilayer and blend films with 3,4,9,10-perylenetetracarboxylic bisbenzimidazole (PTCBI). In all cases, the electrodes (M) were either ITO or Ag, I_P was a 200 nm thick layer of either poly(methyl methacrylate) (PMMA) or PC, and I_{IL} was either MB or TT. Figure 2 shows the RBP comparison for $MI_{IL}SM$ and $MI_{IL}SI_PM$ devices, together with their absolute values of responsivity and bandwidth.

In most cases, the $MI_{IL}SI_PM$ architecture yields a significant improvement in RBP, compared to $MI_{IL}SM$. Notably, in the case of the single layer devices (Dev. 1–3), the improvement in RBP can be up to 1–2 orders of magnitude, owing to a similar responsivity at square wave, coupled with a significantly improved device bandwidth, in comparison to the blend or bilayer devices, where only a negligible or small improvement in RBP can be seen, respectively. Here, it is reasoned that the EDL, which can provide a sufficient energetic interface for charge separation[17,21], yields a more dominant effect in the single active layer devices (Dev. 1–3) due to the absence of any other such energetic interface, *e.g.* a heterojunction or rectifying M/S contact, as are present in the bilayer/blend devices, and the MISM devices, respectively. The function of the EDL seems preserved in $MI_{IL}SI_PM$ devices,
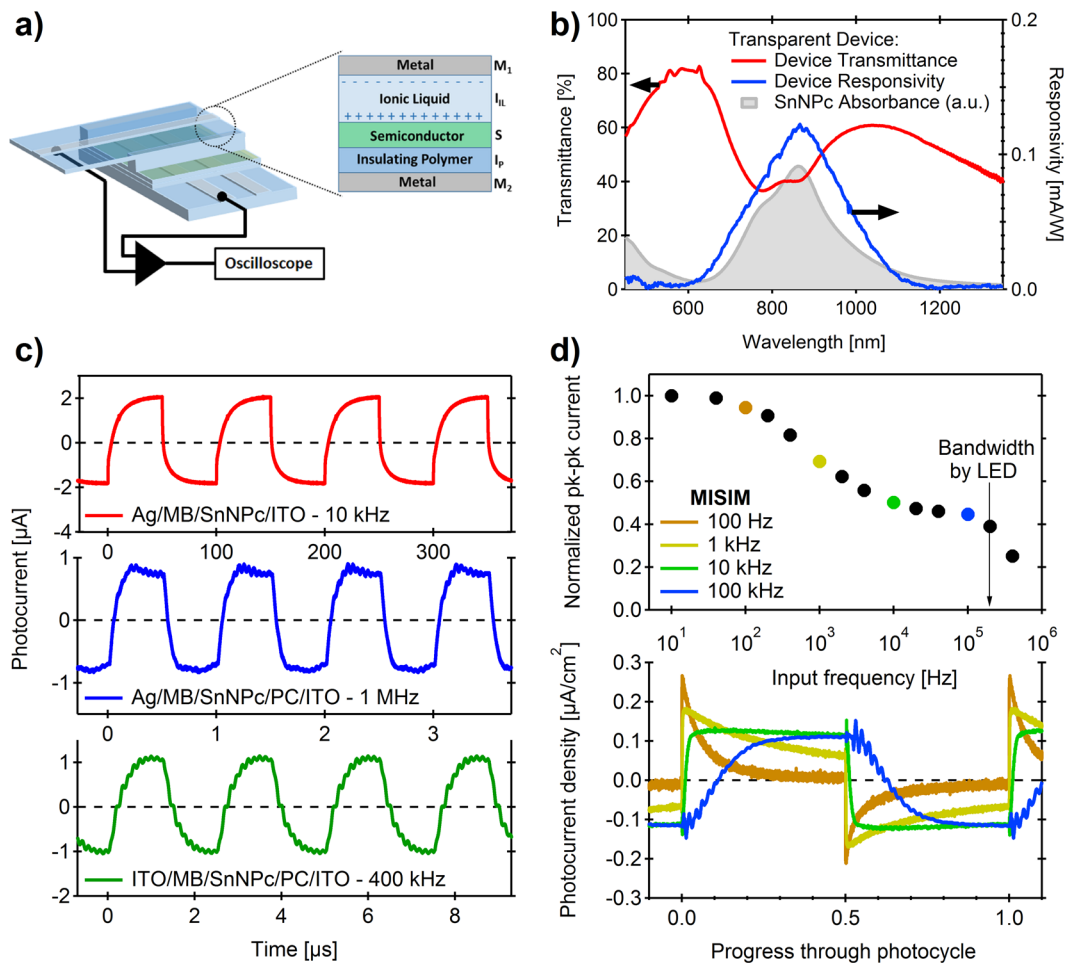
Figure 1. (a) Generalized structure of the $M_1I_{IL}SI_PM_2$ devices used in this study ($M_1I_{IL}SM_2$ devices are identical, except that I_P is absent); (b) responsivity spectrum for the transparent device ($M_1 = M_2 = ITO$, $I_{IL} = MB$, $S = 50\,nm\,SnNPc$, $I_P = 200\,nm\,PC$), compared to the transmission spectrum through the whole device stack. The absorption spectrum of the SnNPc film is shown as the shaded area under the responsivity curve, in arbitrary units, for comparison; (c) photocurrent response for representative $M_1I_{IL}SI_PM_2$ devices, where $M_1 = Ag$ or ITO, compared to $M_1I_{IL}SM_2$ ($M_1 = Ag$) under pulsed laser diode illumination (50% duty cycle, $\lambda = 850\,nm$, $P_{MAX} = 18\,mW$ at 1 MHz, 19 mW at 400 kHz and 34 mW at 10 kHz) at pulse frequencies resulting in an approximately square-wave response; (d) progression of photocurrent response for the $M_1I_{IL}SI_PM_2$ device, where $M_1 = ITO$, under square-wave modulated LED illumination ($\lambda = 850\,nm$, $f = 0.1–100\,kHz$, $P = 1.1\,mWcm^{-2}$).

despite the modified potential drop across the IL with the introduction of the I_P (see further for discussion on the built-in potentials in $MI_{IL}SI_PM$). Therefore, the dominant effect of I_P is to reduce the series capacitance of the device, which manifests itself not just in the decay time of the photocurrent transient, but also in the photocurrent rise time[17]. An additional advantage of the $MI_{IL}SI_PM$ structure is that the polymeric insulator layer can be used as a spacer to move the semiconductor away from the electrode to mitigate against the diminishing optical electric field close to reflective electrode contacts (optical interference effect)[22,23]. This perhaps accounts for the similar responsivity between $MI_{IL}SM$ and $MI_{IL}SI_PM$ in Device 2 which, in turn, affords the largest improvement in RBP.

Interestingly, the $MI_{IL}SI_PM$ architecture yields a similar device bandwidth, regardless of the semiconductor layer arrangement used. This is distinct from the $MI_{IL}SM$ devices, which show a strong dependence of bandwidth with the semiconductor layer structure employed. This suggests that the introduced I_P layer constitutes the smallest capacitive element in the $MI_{IL}SI_PM$ devices, and thus dominates C_{rise}. Furthermore, it should be noted that for all MISIM devices it is the more mobile charge carrier (holes for SnNPc and electrons for PTCBI) that are accumulated at the S/I_{IL} interface, regardless of the electrode arrangement used (in contrast to the MISM analogues), opening a question on the role and orientation of the built-in potentials in the MISIM devices - a question which requires further studies. This unipolar movement of charge solves an outstanding issue for the MISM photodetectors where, for certain active layer arrangements, a bipolar (double peak) response can occur during the light on and off period[21]. Such double peak behaviour has occurred in MISM devices based on single layers, bilayers and bulk heterojunction devices for various active layer materials[24,25]. While this double peak has been used by
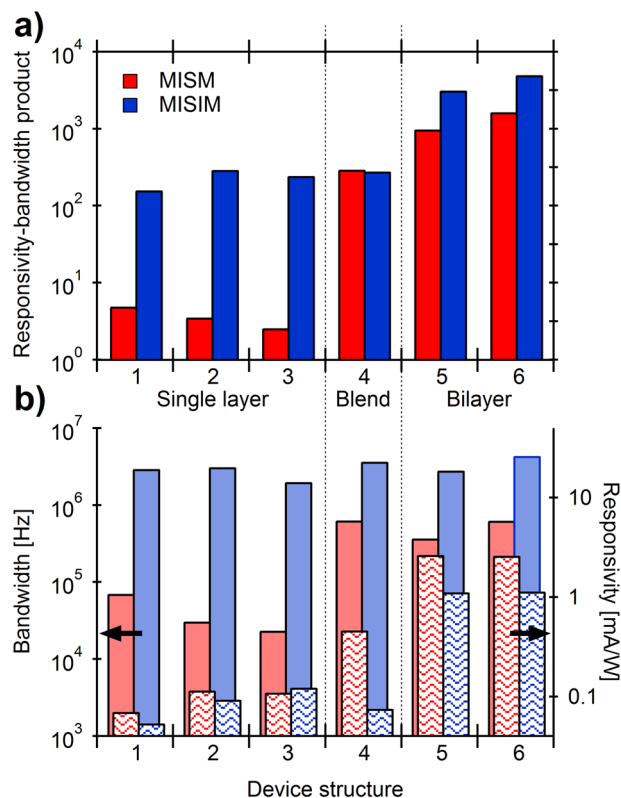
Figure 2. (**a**) Responsivity-bandwidth product (RBP) comparison of $MI_{IL}SM$ and $MI_{IL}SI_PM$ devices for various semiconductor layer arrangements based on SnNPc as a single layer (Dev. 1–3), as a blend (Dev. 4) and as a bilayer (Dev. 5–6) with PTCBI. Dev 1 (see also Fig. 1): ITO/(PC)/SnNPc(50 nm)/MB/Ag; Dev 2: ITO/MB/SnNPc(50 nm)/(PC)/Ag; Dev 3: ITO/(PMMA)/SnNPc(60 nm)/TT/Ag; Dev 4: ITO/(PMMA)/SnNPc:PTCBI(2:1,60 nm)/TT/Ag; Dev 5: ITO/(PC)/SnNPc(40 nm)/PTCBI(20 nm)/MB/Ag; Dev 6: ITO/MB/SnNPc(40 nm)/PTCBI(20 nm)/(PC)/Ag; (**b**) separate values of responsivity and bandwidth for the same devices.

Gautam *et al.* as the basis for an elegant colour-sensitive detector[26], this effect generally comes at the expense of device responsivity.

From Fig. 2 it can be seen that the bilayer devices show the highest values of RBP for all of the architectures tested. However, the requirement of finding a suitable heterojunction partner, which becomes harder for lower bandgap absorbers, imposes a limit on this architecture as a general strategy for near-infrared photodetection. Due to the pronounced increases in RBP for the single layer devices, we sought to explore methods to further improve the performance of $MI_{IL}SI_PM$ based on single component semiconductor layers by decreasing the series resistance of the active layer. Based on previous work, such a strategy can be expected to yield a simultaneous improvement in the device bandwidth and responsivity[17].

A key advantage of differential photodetector devices (both MISM and MISIM) is their ability to operate under strong background light conditions, since the devices are only sensitive to changes in light intensity, rather than the light intensity itself[17]. Under such conditions, a decrease in the series resistance component of the active layer could be expected due to an increased charge carrier density through pre-illumination of the semiconductor layer. As a proof of principle, the pure semiconductor device (Dev. 3 from Fig. 2) was tested under continuous wave (CW) laser illumination at 10% modulation depth ($f = 2$ MHz, P = 14 mW, $P_{mod} = 1.4$ mW), and the response compared to that obtained by the pulsed laser (P = 28 mW), as shown in Fig. 3. It is clear from the lack of photocurrent offset (photocurrent oscillates around zero) that the device operates as a differentiator, even at high background light intensities. Furthermore, under modulated CW illumination, the rise time falls by a factor of 1.3 to 90 ns (BW = ~3.9 MHz), while the responsivity increases 5x, thereby demonstrating that a reduced active layer resistance strongly improves device performance despite an expected loss in responsivity resulting from optical saturation. As a result, the device shows a 6.6x improvement in RBP to over 1000.

An alternative strategy to decrease the series resistance of the active layer, uniquely applicable to MISM or MISIM devices, was to blend directly the semiconductor with a conductive element. To effect this, a blend film of SnNPc with Au was deposited by co-evaporation, and the photoresponse compared to that of a pure SnNPc layer of identical thickness (Dev. 3 in Fig. 2) (Fig. 4a). As can be seen, the co-deposited device shows a > 2-fold improvement in photocurrent response at square-wave, while the rise time is simultaneously shortened by a factor of 1.5 to 81 ns (BW = ~4.3 MHz), yielding a RBP of 580, approaching the values obtained for the bilayer devices. It should be noted that, in contrast to the other devices in Fig. 2, where the absorption intensity at 850 nm were broadly similar, the SnNPc:Au film showed a ~2-fold reduction in absorption compared to Device 3 (see Supplementary Fig. S1). Thus using the internal quantum efficiency as a basis of comparison might be more
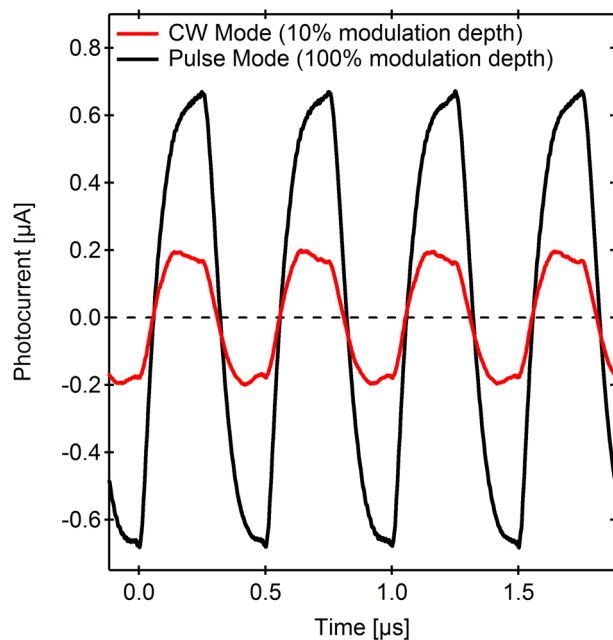
Figure 3. Photocurrent waveforms for Device 3, (see also Fig. 2) measured at 2 MHz using pulsed laser light illumination (50% duty cycle, $P = 28$ mW), compared to square-wave modulated CW laser light ($P = 14$ mW, $P_{Mod} = 1.4$ mW) at 10% modulation depth.
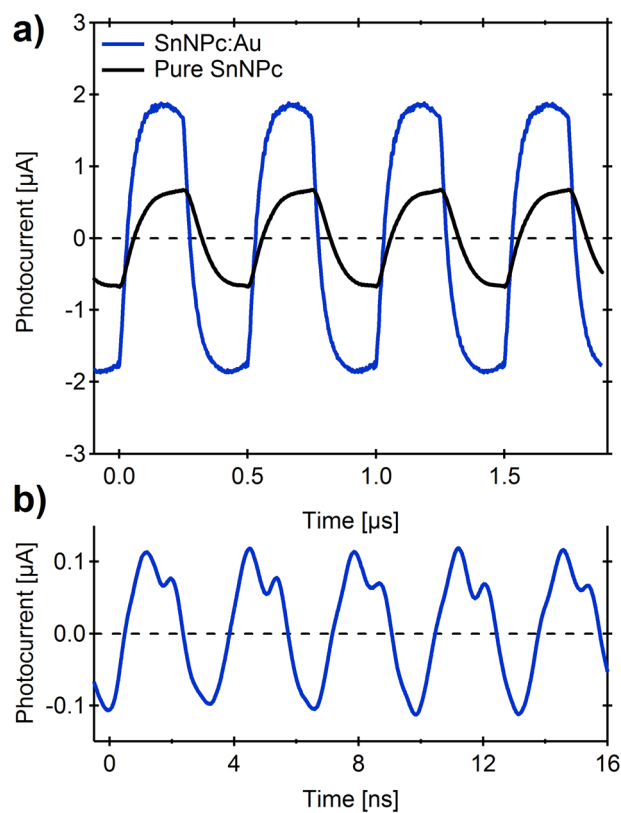
Figure 4. (**a**) Comparison of photocurrent waveforms for $MI_{IL}SI_{P}M$ devices based on SnNPc (Dev. 3) and SnNPc:Au as the semiconductor layer, measured at 2 MHz using pulsed laser light illumination (50% duty cycle, $\lambda = 850$ nm, $P = 28$ mW); (**b**) photocurrent response for SnNPc:Au device measured at 300 MHz using pulsed laser light illumination (20% duty cycle, $\lambda = 850$ nm, $P = 21$ mW).

informative in such instances. Figure 4b shows that this device is also capable of clearly resolving optical signals at frequencies up to 300 MHz (thus, far beyond its bandwidth), since the photocurrent offset is intrinsically zero, allowing signal amplification without amplifier overload. While it is premature to attribute this device improvement solely to the reduced series resistance of the device (since improved light harvesting through scattering and/or plasmonic effects might also play a role[27–29]), these results are consistent with previous work for spin-coated active layer films with incorporated carbon black[18], and suggests metallic blending of the semiconductor layer to be a viable and general route to further improve differential photodetection. It should be noted that operating this device under CW modulation shows only negligible improvement in RBP to 620, as might be expected for an already low resistance semiconducting layer.

In this study, a general strategy to improve the device bandwidth for ionic liquid-functionalized differential photodetectors is demonstrated by adopting a $MI_{IL}SI_PM$ architecture, where I_P is a low-k polymer dielectric. The operating mechanism for such devices is based purely on the polarization of the active layer under illumination, requiring no carrier injection from the electrodes. While a photoresponse based on pure polarization can also be achieved using two polymer dielectrics (see Supplementary Fig. S2), where electrochemistry, chemical doping and active layer dissolution are unquestionably absent, the increases in bandwidth are counterbalanced by a comparably strong decrease in responsivity, and thus the overall improvement in RBP is less pronounced than in the $MI_{IL}SI_PM$ system. It should be noted, that by choosing the right ionic liquid for the specific active layer, a stable photocurrent response, with minimal degradation or baseline drift, can be achieved. For single layer and bilayer semiconductor systems, the improvement in bandwidth in the $MI_{IL}SI_PM$ devices is larger than the loss in responsivity caused by a reduced total insulator capacitance, thus resulting in a net gain in responsivity-bandwidth product compared to $MI_{IL}SM$ for both these active layer arrangements. A further optimization of single component semiconductor devices is also demonstrated by reducing the series resistance of the semiconductor through operation of the device under strong background light, as well as through semiconductor:metal blending. By demonstrating device bandwidths of 4 MHz, even for a low mobility semiconductor, this study paves the way for >MHz photodetection from those organic dyes that have previously been deemed unsuitable for such purposes, but that otherwise show desirable absorption properties. Work is ongoing to assess the effect of semiconductor and insulator layer thickness on device performance, as well as the role of the built-in potentials from the outer electrode materials. In addition, improvements in both responsivity and bandwidth for $MI_{IL}SI_PM$ devices will be targeted through the use of higher mobility and stronger chromophoric semiconductors, in an effort to tune the RC component of the photoactive semiconductor layer.

Methods
Further information on all the fabrication and testing methods can be found in the Supplementary Information.

Fabrication Methods. *General Methods.* All substrates were cleaned by mild bath ultrasonnication ($P = 45$ W, 0.5% Helmanix III solution, acetone, methanol, 10 mins each) and blown dry with nitrogen. Unless otherwise stated, all substrates were further subjected to UV/air plasma cleaning (Bioforce Nanosciences ProCleanerPLUS, 10 mins.) immediately prior to deposition (excepting Ag electrodes, which were freshly deposited before use).

PMMA (Mw = 350,000 – Sigma Aldrich) was spin coated from a solution of chlorobenzene (4 wt.%), and annealed on a hotplate at 160 °C for 10 mins. Parylene-C (SCS) was deposited using a Specialty Coating Systems PDS2010 deposition unit.

Organic semiconductors (SnNPc – Sigma Aldrich, PTCBI – synthesised according to Mamada *et al.*[30]) and metals (Ag, Au) were deposited by physical vapour deposition at a base pressure of $<4 \times 10^{-4}$ Pa by resistive heating of ceramic crucibles or tungsten boats, respectively. Growth rates were (independently) monitored by quartz crystal microbalance(s), and film thicknesses were validated by surface profilometry (Dektak 150).

Thin-film absorption measurements (Shimadzu UV-3100PC) were recorded on quartz substrates in transmission mode. For the device transmission measurement, a perforated plate of $\emptyset = 1.0$ mm was used to ensure the incident light passed through the patterned ITO electrode.

Device Fabrication. Semiconductor films were deposited on patterned electrode (Ag or ITO) substrates (15×15 mm (substrate) with 2 mm wide electrode strips), either with or without a 200 nm film of polymer dielectric (PMMA or Parylene-C). The devices were assembled in a stacked architecture, where the counter electrode (either unpatterned ITO on a 10×20 mm glass substrate, or a 2 mm wide strip of Ag on glass of the same dimensions) was fixed on top and perpendicular to the active layer electrode with a thermally sealable 60 μm Surlyn spacer (Solaronix), as shown in Fig. 1a. The void between the electrodes was filled with ionic liquid (either *N*-(2-methoxyethyl)-*N*-methylpyrrolidinium tetrafluoroborate (MB) received as a gift from Nisshinbo Holdings Inc., or trimethylpropylammonium bis(trifluoromethanesulfonyl)imide (TT) (Kanto Chemicals)).

Device Testing. *Frequency dependent photocurrent measurements.* For LED measurements, the LED light ($\lambda_{max} = 850$ nm) was directed onto a collimator via an optical fibre, resulting in a 7 mm homogeneous broad beam, which was modulated as a square-wave light signal by a function generator (Tektronix AWG2041). In all cases, the light power was adjusted to $P_{incident} \approx 1.1$ mWcm^{-2}, and the responsivity was calculated based on a device area ≈ 0.14 cm^2 (ITO width × beam diameter).

For pulsed laser measurements, a customised laser (spot size = 2×1 mm, $\lambda_{max} = 848 \pm 10$ nm, OPG-1000PL-850, Scientex) was used to generate pulsed light signals of approximately square-wave shape with a duty cycle of about 50% over a frequency range of 10 kHz to 1 GHz, controlled by a function generator (Tektronix AWG2041) (see Supplemental Fig. SX1).

For CW laser measurements, the same laser was used for generating a modulated CW waveform (using the CW trigger input). In this case, the laser power was linearly set by the laser input power (0–100%), with a constant modulation of about 10% of the maximum laser power (*i.e.* at an input power = 100%) for a laser power over 10% (see Supplemental Fig. SX2).

In all cases the generated photocurrent response was amplified using a high-speed transimpedance amplifier (Femto DHPCA100 (up to 10 MHz), or Femto HSA-Y-1-60 (2 MHz–300 MHz)), and visualized on an oscilloscope (Tektronix TDS5104B) in high resolution or average mode. The signals were displayed, so that a positive peak corresponds to the light on signal. In the case of the responsivity-bandwidth product (RBP), the responsivity was calculated using the pk-pk value of the photocurrent response for a square-wave device signal recorded at an appropriate modulation frequency, while the bandwidth was estimated from the rise time of this square-wave signal, as described in the manuscript above.

Wavelength dependent measurements. The devices were illuminated by a tungsten/halogen light source (Spectral Products ASBN-W 100 L) attached to a monochromator (Digikröm CM110, slits 1.2 and 0.6 mm, resolution 8–10 nm), and modulated by a chopper (NF Corp. 5584 A). The photocurrent signals were extracted using a lock-in amplifier (NF 5610B/A), pre-amplified using a low noise transimpedance amplifier (Femto, DLPCA 200) and recorded on a computer. The setup was controlled by a home-written LabVIEW program, scanning the wavelength range from 1400 to 400 nm (step ± 2 nm at 2 s/step). The responsivity spectra were determined by dividing the photocurrent spectra by the wavelength-dependent light power (see Supplementary Fig. SX3).

Data Availability

The datasets generated during and/or analysed during the current study are available from the corresponding author on reasonable request.

References

1. Jansen-van Vuuren, R. D., Armin, A., Pandey, A. K., Burn, P. L. & Meredith, P. Organic photodiodes: the future of full color detection and image sensing. *Advanced Materials* **28**, 4766–4802 (2016).
2. Baeg, K.-J., Binda, M., Natali, D., Caironi, M. & Noh, Y.-Y. Organic light detectors: photodiodes and phototransistors. *Advanced Materials* **25**, 4267–4295 (2013).
3. Kröger *et al.* Role of the deep-lying electronic states of MoO₃ in the enhancement of hole-injection in organic thin films. *Applied Physics Letters* **95**, 123301 (2009).
4. Kotadiya *et al.* Universal strategy for Ohmic hole injection into organic semiconductors with high ionization energies. *Nature Materials* **17**, 329–334 (2018).
5. Brabec, C. J., Shaheen, S. E., Winder, C. & Sariciftci, N. S. Effect of LiF/metal electrodes on the performance of plastic solar cells. *Applied Physics Letters* **80**, 1288 (2002).
6. Huang, J., Li, G. & Yang, Y. A semi-transparent plastic solar cell fabricated by a lamination process. *Advanced Materials* **20**, 415–419 (2008).
7. Zhou, Y. *et al.* A universal method to produce low-workfunction electrodes for organic electronics. *Science* **336**, 327–332 (2012).
8. Bergqvist, J. *et al.* Asymmetric photocurrent extraction in semitransparent laminated flexible organic solar cells. *npj Flexible Electronics* **2**, 4 (2018).
9. Ferenczi, T. A. M. *et al.* Organic semiconductor:insulator polymer ternary blends for photovoltaics. *Advanced Materials* **23**, 4093–4097 (2011).
10. Huang, Y. *et al.* High-molecular-weight insulating polymers can improve the performance of molecular solar cells. *Advanced Materials* **26**, 4168–4172 (2014).
11. Lin, C.-H. & Liu, C. W. Metal-insulator-semiconductor photodetectors. *Sensors* **10**, 8797–8826 (2010).
12. Binda, M. *et al.* High detectivity squaraine-based near infrared photodetector with nA/cm⁻² dark current. *Applied Physics Letters* **98**, 073303 (2011).
13. Kielar, M., Dhez, O., Pecastaings, G., Curutchet, A. & Hirsch, L. Long-term stable organic photodetectors with ultra low dark currents for high detectivity applications. *Scientific Reports* **6**, 39201 (2016).
14. Yao, Y. *et al.* Plastic near-infrared photodetectors utilizing low band bap polymer. *Advanced Materials* **19**, 3979–3983 (2007).
15. Gong, X. *et al.* High-detectivity polymer photodetectors with spectral response from 300 nm to 1450 nm. *Science* **325**, 1665–1667 (2009).
16. Hu, L. *et al.* Organic optoelectronic interfaces with anomalous transient photocurrent. *Journal of Materials Chemistry C* **3**, 5122–5135 and references therein (2015).
17. Reissig, L., Dalgleish, S. & Awaga, K. A differential photodetector: detecting light modulations using transient photocurrents. *AIP Advances* **6**, 015306 (2016).
18. Dalgleish, S. *et al.* Utilizing photocurrent transients for dithiolene-based photodetection: stepwise improvements at communications relevant wavelengths. *Journal of the American Chemical Society* **134**, 12742–12750 (2012).
19. Li, B. *et al.* Electric double layers allow for opaque electrodes in high performance organic optoelectronic devices. *Applied Physics Letters* **101**, 173302 (2012).
20. Hu, L. *et al.* Optoelectronic conversion by polarization current, triggered by space charges at organic-based interfaces. *Applied Physics Letters* **96**, 243303 (2010).
21. Dalgleish, S. *et al.* Controlling the crystallinity and crystalline orientation of "shuttlecock" naphthalocyanine films for near-infrared optoelectronic applications. *Journal of Materials Chemistry C* **6**, 1959–1970 (2018).
22. Kim, J. Y. *et al.* New architecture for high-efficiency polymer photovoltaic cells using solution-based titanium oxide as an optical spacer. *Advanced Materials* **18**, 572–576 (2006).
23. Park, S. H. *et al.* Bulk heterojunction solar cells with internal quantum efficiency approaching 100%. *Nature Photonics* **3**, 297–303 (2009).
24. Reissig, L., Mori, K., Treadwell, R., Dalgleish, S. & Awaga, K. Factors affecting the polarity and magnitude of photoresponse of transient photodetectors. *Physical Chemistry Chemical Physics* **18**, 6821–6830 (2016).
25. Gautam, V., Bag, M. & Narayan, K. S. Dynamics of bulk polymer heterostructure/electrolyte devices. *Journal of Physical Chemistry Letters* **1**, 3277–3282 (2010).
26. Gautam, V., Bag, M. & Narayan, K. S. Single-pixel, single-layer polymer device as a tricolor sensor with signals mimicking natural photoreceptors. *Journal of the American Chemical Society* **133**, 17942–17949 (2011).
27. Qu, D., Liu, F., Huang, Y., Xie, W. & Xu, Q. Mechanism of optical absorption enhancement in thin film organic solar cells with plasmonic metal nanoparticles. *Optics Express* **19**, 24795–24803 (2011).

7

28. Baek, S.-W. *et al*. Plasmonic forward scattering effect in organic solar cells: a powerful optical engineering method. *Scientific Reports* **3**, 1726 (2013).
29. Hou, J.-L. *et al*. Plasmon-induced sub-bandgap photodetection with organic schottky diodes. *Advanced Functional Materials* **26**, 5741–5747 (2016).
30. Mamada, M., Pérez-Bolívar, C. & Anzenbacher, P. Jr. Green synthesis of polycyclic benzimidazole derivatives and organic semiconductors. *Organic Letters* **13**, 4882–4885 (2011).

Author Contributions
L.R. and S.D. conceived the idea of the MISIM photocell. S.D. developed the method of metal:semiconductor blending. L.R. and S.D. designed and conducted all the mentioned experiments, as well as analysed and interpreted the data. All authors contributed to the discussion of the results and the writing of the manuscript.

Additional Information
Supplementary information accompanies this paper at https://doi.org/10.1038/s41598-018-33822-z.

Competing Interests: The authors declare no competing interests.

Publisher's note: Springer Nature remains neutral with regard to jurisdictional claims in published maps and institutional affiliations.